Inhibition of myeloperoxidase-mediated protein nitration by tempol: Kinetics, mechanism, and implications

Sandra M. Vaz and Ohara Augusto*

Departamento de Bioquímica, Instituto de Química, Universidade de São Paulo, Caixa Postal 26077, CEP 05513-970 São Paulo, Brazil

Edited by Joan Selverstone Valentine, University of California, Los Angeles, CA, and approved March 14, 2008 (received for review, August 30, 2007)

Despite the therapeutic potential of tempol (4-hydroxy-2,2,6,6-tetra-methyl-1-piperidinyloxy) and related nitroxides as antioxidants, their effects on peroxidase-mediated protein tyrosine nitration remain unexplored. This posttranslational protein modification is a biomarker of nitric oxide-derived oxidants, and, relevantly, it parallels tissue injury in animal models of inflammation and is attenuated by tempol treatment. Here, we examine tempol effects on ribonuclease (RNase) nitration mediated by myeloperoxidase (MPO), a mammalian enzyme that plays a central role in various inflammatory processes. Some experiments were also performed with horseradish peroxidase (HRP). We show that tempol efficiently inhibits peroxidase-mediated RNase nitration. For instance, 10 μM tempol was able to inhibit by 90% the yield of 290 μM 3-nitrotyrosine produced from 370 μM RNase. The effect of tempol was not completely catalytic because part of it was consumed by recombination with RNase-tyrosyl radicals. The second-order rate constant of the reaction of tempol with MPO compound I and II were determined by stopped-flow kinetics as 3.3×10^6 and 2.6×10^4 M^{-1} s^{-1}, respectively (pH 7.4, 25°C); the corresponding HRP constants were orders of magnitude smaller. Time-dependent hydrogen peroxide and nitrite consumption and oxygen production in the incubations were quantified experimentally and modeled by kinetic simulations. The results indicate that tempol inhibits peroxidase-mediated RNase nitration mainly because of its reaction with nitrogen dioxide to produce the oxammonium cation, which, in turn, recycles back to tempol by reacting with hydrogen peroxide and superoxide radical to produce oxygen and regenerate nitrite. The implications for nitroxide antioxidant mechanisms are discussed.

antioxidant | tyrosine | tyrosine nitration | nitroxides | nitric oxide-derived oxidants

Despite the substantial evidence indicating that oxidative mechanisms contribute to the pathogenesis of many human diseases, multiple large prospective intervention trials with classical antioxidants such as vitamin C, vitamin E and β-carotene failed to have a significant impact on disease risk and progression (1, 2). Among the many reasons responsible for such inconclusive results, we may include incomplete knowledge of the chemical biology of redox processes and limited actions of classical antioxidants (2, 3). The need to translate the basic information about cellular redox processes gained in the past 40 years into clinical applications justifies a better understanding of the properties of nonclassical antioxidants such as cyclic nitroxides (4). Indeed, tempol and other stable nitroxide radicals have long been known to protect laboratory animals from injuries associated with a variety of oxidative stress conditions. Moreover, these compounds are multifunctional antioxidants because they react with diverse biological oxidants and reductants while being recycled through oxammonium cation ($TPNO^+$) and hydroxylamine derivatives (TPNOH), respectively (Eq. **1**) (reviewed in refs. 5 and 6). Eventually, nitroxides can be consumed by recombination reactions with certain radicals, such as thiyl radicals (Eq. **2**) (6, 7).

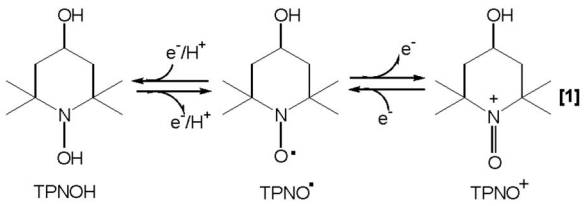

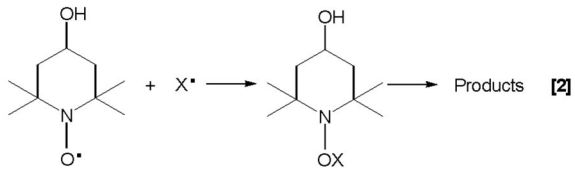

The most cited antioxidant mechanism of nitroxides is their superoxide dismutase activity, probably because it was the first property described at the molecular level (8). However, nitroxides are not particularly efficient SOD mimetics (9) and are unlikely to surpass SOD isoenzymes, which are abundant in most physiological compartments. Other nitroxide antioxidant mechanisms include inhibition of Fenton chemistry by the ability to oxidize transition metal ions, termination of radical chain reactions by radical recombination (Eq. **2**), and acceptance of electrons from mitochondrial electron transport chains (5, 6). The possibility of cyclic nitroxides interacting with $NO^{\bullet}$-derived oxidants has been investigated less frequently (7, 9–13). Nevertheless, this is particularly relevant because tempol has also been shown to protect animals from injuries associated with inflammatory conditions that are characterized by increased production of $NO^{\bullet}$ and its derived oxidants (reviewed in ref. 14). Because $NO^{\bullet}$-derived oxidants promote Tyr nitration (15), it is not surprising that the protective effects of tempol in animal models of inflammation are paralleled by decreased levels of protein-tyrosine nitration.

Protein-tyrosine nitration is attracting considerable attention from biomedical investigators because of its potential ability to alter protein function, indicate acute and chronic disease states, and predict disease risk. Although biological nitration can occur at Tyr and Trp residues, lipids, and nucleic acid bases, Tyr nitration has attracted most attention because of its high occurrence in proteins and the sensitive detection of 3-nitrotyrosine in biological samples by immunological techniques (reviewed in ref. 15).

Author contributions: S.M.V. and O.A. designed research; S.M.V. performed research; S.M.V. and O.A. analyzed data; and O.A. wrote the paper.

The authors declare no conflict of interest.

This article is a PNAS Direct Submission.

*To whom correspondence should be addressed. E-mail: oaugusto@iq.usp.br.

This article contains supporting information online at www.pnas.org/cgi/content/full/0708211105/DCSupplemental.

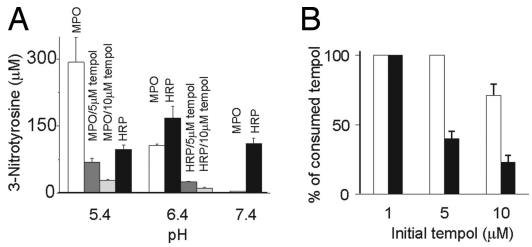

Fig. 1. Inhibition of peroxidase-mediated RNase nitration by tempol. (*A*) Production of 3-nitrotyrosine in RNase (370 μM) after 40 or 60 min incubation with 1 mM H_2O_2, 1 mM NO_2^-, and either 30 nM (10 units/ml) MPO or 10 μM (450 units/ml) HRP, respectively, in the absence or presence of tempol in 50 mM phosphate at the specified pH and 37°C. (*B*) Percentage of tempol consumed as a function of the initial tempol concentration in the above incubation mixtures containing MPO at pH 5.4 (open bars) or HRP at pH 6.4 (filled bars). Tempol consumption was monitored by the decay of its EPR spectrum. Shown values are average ± SD of three independent experiments.

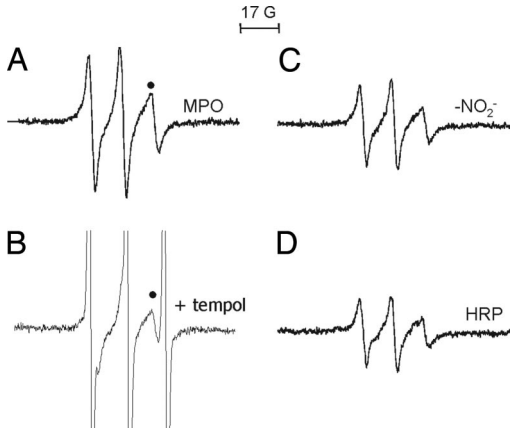

Fig. 2. Peroxidase-mediated production of RNase-tyrosyl radical. (*A*) EPR spectrum obtained after a 10-min incubation of the standard incubation mixture (370 μM RNase, 30 nM (10 units/ml) MPO, 1 mM H_2O_2, 1 mM NO_2^-, pH 5.4 and 37°C) in the presence of 10 mM DBNBS. (*B*) Same as *A*, in the presence of 10 μM tempol. (*C*) Same as *A*, in the absence of NO_2^-. (*D*) EPR spectrum obtained after 30-min incubation of the standard HRP mixture (370 μM RNase, 10 μM (450 units/ml) HRP, 1 mM H_2O_2, 1 mM NO_2^-, pH 6.4 and 37°C) in the presence of 10 mM DBNBS. The point marks the spectrum line used to estimate tempol inhibition of DBNBS/•tyrosyl-protein radical adduct yield. Instrumental conditions: microwave power, 20 mW; time constant, 327.7 ms; sweep time, 335.5 s; modulation amplitude, 1.0 G; receiver gain, 1.26×10^5.

The better elucidated protein-tyrosine nitration mechanism supports a radical recombination of $NO_2^\bullet$ with protein-tyr$^\bullet$ to produce 3-nitrotyrosine residues. Not unexpectedly, efficient Tyr nitration has been demonstrated so far with systems that directly or indirectly produce Tyr$^\bullet$ in addition to $NO_2^\bullet$. Examples of such systems are hemeperoxidases/H_2O_2/NO_2^- and peroxynitrite/CO_2 (4, 15). In the presence of H_2O_2, hemeperoxidases such as myeloperoxidase form compounds I (MPO-I, $E^\circ = 1.35$ V) and II (MPO-II, $E^\circ = 0.97$ V) (16) which can oxidize both NO_2^- and Tyr to $NO_2^\bullet$ and Tyr$^\bullet$, respectively. In the case of peroxynitrite/CO_2, these components react quickly to produce $NO_2^\bullet$ and $CO_3^{\bullet-}$ in 35% yield. A simultaneous flux of these radicals is efficient in nitrating Tyr because the highly oxidizing $CO_3^{\bullet-}$ produces Tyr$^\bullet$ that recombines with $NO_2^\bullet$ (4, 15). Because tempol reacts rapidly with both $NO_2^\bullet$ and $CO_3^{\bullet-}$ (11–13), it is not surprising that it inhibited peroxynitrite/CO_2-mediated nitration of phenol (10) and BSA and cell proteins (7).

The effects of cyclic nitroxides on hemeperoxidase-mediated protein nitration, however, remained unexplored. Nitroxides have been shown to react with the ferryl states produced from myoglobin, hemoglobin, HRP/phenol, and lactoperoxidase/phenol, facilitating their catalase activity (17, 18). However, these systems are unlikely to be relevant for pathophysiological protein nitration under most circumstances. Here, we examine the kinetics and mechanisms of tempol inhibition of protein-tyrosine nitration, mediated by MPO, a mammalian enzyme that plays a central role in innate immune defense and various inflammatory processes (reviewed in refs. 16, 19, and 20). For comparative purposes, some experiments were also performed with HRP. The nitration target used was RNase, a model protein that contains 6 Tyr, no Trp, and all of 8 Cys involved in intramolecular disulfide bonds (21).

Results

Inhibition of Peroxidase-Mediated RNase Nitration by Tempol. RNase has been previously used as a target of MPO-mediated nitration at pH 7.4 (21). Here, we examined the production of 3-nitrotyrosine in RNase treated with 1 mM H_2O_2, 1 mM NO_2^-, and either 30 nM MPO or 10 μM HRP at pH 5.4, 6.4, and 7.4 (Fig. 1*A*). MPO-mediated RNase nitration was strongly enzyme- and pH-dependent. Although less sensitive to pH, HRP-mediated nitration was higher at pH 6.4. MPO efficiency in promoting RNase nitration is clear because, at pH 5.4, nanomolar MPO produced almost three times more 3-nitrotyrosine residues than micromolar HRP (Fig. 1*A*). Stoichiometrically, MPO promoted the nitration of almost one Tyr residue (290 μM) per RNase molecule (370 μM) at pH 5.4. Parallel production of lower yields of 3-hydroxytyrosine and dityrosine was proven by HPLC analysis of trypsin hydrolysates of treated RNase; the main oxidized/nitrated residues were those present in the peptides containing $Tyr^{92/97}$ and $Tyr^{73/76}$ [see supporting information (SI) Fig. S1]. To examine tempol effects, however, only overall RNase nitration yield was monitored. MPO-mediated RNase nitration was almost completely inhibited by low micromolar concentrations of tempol (5–10 μM) (Fig. 1*A*). Likewise, tempol strongly inhibited HRP-mediated nitration. Tempol inhibitory effects were observed under all tested conditions of measurable RNase nitration, but most of the subsequent experiments were performed at pH values that yielded maximum nitration, that is, pH 5.4 and 6.4 for MPO and HRP, respectively. Protein nitration at low pH is relevant because acidic environments can be found at cell surfaces, phagolysosomes of phagocytic cells, and ischemic tissues.

The low tempol concentrations (5–10 μM) required to extensively inhibit RNase nitration suggested that it might be acting catalytically. However, depending on its initial concentration, tempol was totally or partially consumed, as monitored by the EPR spectra of the final incubation mixtures (Fig. 1*B*). In incubations containing MPO, tempol was completely consumed in those that started with 1 or 5 μM tempol, whereas ≈3 μM remained in incubations that started with 10 μM tempol. One possibility to explain tempol consumption was recombination reactions with RNase-tyr$^\bullet$ (Eq. **2**) (7, 22). To test this possibility, we examined radical production by EPR spin-trapping experiments with 3,5-dibromo-4-nitrosobenzenesulfonate (DBNBS). Incubations of RNase with MPO/H_2O_2/NO_2^- in the presence of DBNBS produced a spectrum whose EPR parameter (a_N = 13.7 G) (Fig. 2*A*) was consistent with a DBNBS/•tyr-protein radical adduct because RNase has no Trp residue (23). The obtained spectrum was relatively mobile, indicating that solvent-exposed Tyr residues are being oxidized by MPO/H_2O_2/NO_2^-. Interestingly, the yield of the DBNBS/•tyr-protein radical adduct was significant even in the absence of NO_2^- (Fig. 2*C*), demonstrating that RNase-tyr$^\bullet$ formation does not necessarily require $NO_2^\bullet$ production. Despite the relative inaccessibility of the MPO active site, the enzyme has been shown to oxidize Tyr residues in a synthetic polypeptide containing a high Tyr content (20%) (24). Most likely, MPO oxidizes RNase-tyrosine residues

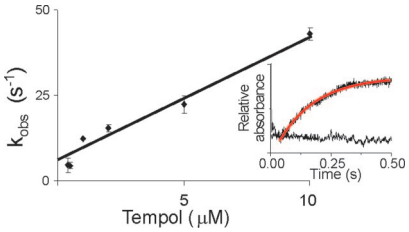

Fig. 3. Determination of the second-order rate constant value for the reaction of tempol with MPO-I. Pseudo first-order rate constants were determined on premixing 0.2 μM MPO with 4 μM H_2O_2 in 0.1 M phosphate buffer, pH 7.4. After a delay time of 0.1 s, formed MPO-I was allowed to react with the specified tempol concentrations, which were in 10-fold excess of MPO-I but not too high to preclude attainment of steady-state conditions. The reaction time course was monitored at 456 nm and *Inset* shows a typical trace (black line) and curve fit (red line) obtained with 2 μM tempol. The apparent second-order rate constant was calculated from the slope by using linear least-squares regression analysis.

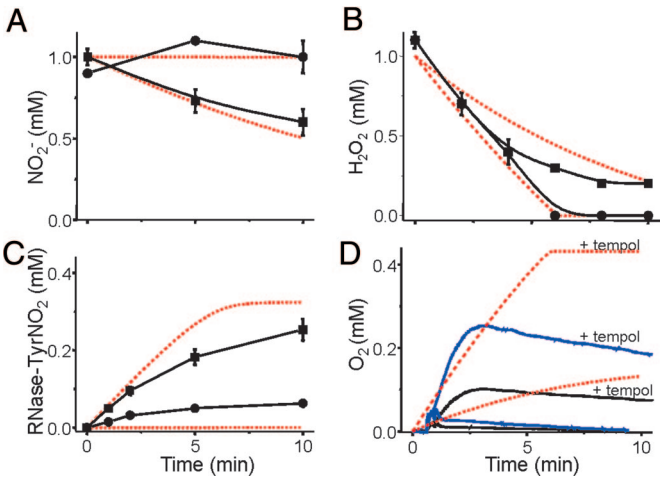

Fig. 4. Experimental (black) and simulated (red) data of tempol effects on the time-dependent substrate consumption and product formation in MPO-containing incubations. The incubations (370 μM RNase, 10 units/ml MPO, 1 mM H_2O_2, 1 mM NO_2^-) were performed at pH 5.4 and 37°C. (*A*) Time-dependent NO_2^- consumption in the absence (filled square) and presence (filled circle) of 10 μM tempol. (*B*) Time-dependent H_2O_2 consumption in the absence (filled square) and presence (filled circle) of 10 μM tempol. (*C*) Time-dependent production of 3-nitrotyrosine in the absence (filled square) and presence (filled circle) of 10 μM tempol. (*D*) Time-dependent O_2 evolution in the absence (unlabeled lines) and presence (labeled lines) of 10 μM tempol by standard incubations except for the use of 0.4 mM H_2O_2. The black curves are experimental data, whereas the blue curves were calculated by multiplying the experimental curves by 2.5. This was necessary to estimate O_2 evolution under our standard condition of 1 mM H_2O_2 (see text). Hydrogen peroxide, NO_2^-, and 3-nitrotyrosine analyses were performed from aliquots submitted to iodometric, chemiluminescence, and spectrophotometric assay, respectively. Shown values are average ± SD of three independent experiments. All red lines correspond to the kinetic simulations modeled with the Gepasi software (see text).

through a MPO-I isomer resulting from electron transfer from its porphyrin cation to an amino acid of its polypeptide chain (24–26). Under our experimental conditions, tempol at an initial concentration of 10 μM inhibited the yield of the DBNBS/•tyr-RNase radical adduct by ≈50%, as shown by comparing the low field line of the radical adduct spectrum (marked in Fig. 2) that does not coincide with tempol spectrum lines. Thus, micromolar tempol competes with millimolar DBNBS for the RNase-tyr•, a fact that is in agreement with the known second-order rate constants of nitroxides and DBNBS reacting with carbon-centered radicals (22). In line with the lower HRP efficiency in nitrating RNase compared with MPO (Fig. 1*A*), tempol consumption (Fig. 1*B*) and RNase-tyr• formation (Fig. 2*D*) were lower in HRP-containing incubations.

Stopped-Flow Kinetics. Although MPO and HRP properties vary markedly, their catalytic peroxidase cycle is similar and involves production of ferryl states (MPO-I and MPO-II and HRP-I and HRP-II) that oxidize different substrates with second-order rate constants that have been determined under a variety of experimental conditions (20, 27). Here, we determined the second-order rate constant of the reaction of tempol with MPO-I (Fig. 3), MPO-II (Fig. S2), HRP-I (Fig. S3) and HRP-II (Fig. S4) by stopped-flow kinetics. The determined second order rate constant values (k) are collected in Table 1 and agree well with reported data that show, for most substrates, k of MPO-I reactions varying between 10^6 and 10^7 M^{-1} s^{-1}, whereas k values of MPO-II, HRP-I, and HRP-II reactions are usually lower and vary more widely (27). The second-order rate constant of the reaction of tempol with MPO-I ($k = 3.3 \times 10^6$ M^{-1} s^{-1}) is high but comparable to that of endogenous substrates. Despite most of our experiments being carried out at 37°C and pH 5.4 and 6.4 for MPO and HRP, respectively, kinetic studies with MPO were performed at pH 7.4 and 25°C to minimize errors because of the possibility of MPO reactions becoming too fast to be monitored in the stopped-flow instrument. Because radical reactions have low activation energies, and HRP reaction rate constant values did not vary significantly at pH 6.4 and 7.4 (Table 1), the determined rate constant values were considered applicable to model tempol effects through kinetic simulations.

Table 1. Values of second-order rate constants determined for tempol reacting with MPO and HRP compound I and II at 25°C*

Reactant	k, M^{-1} s^{-1}	pH
MPO-I	$(3.3 \pm 0.5) \times 10^6$	7.4
MPO-II	$(2.6 \pm 0.7) \times 10^4$	7.4
HRP-I	$(1.2 \pm 0.2) \times 10^3$	6.4, 7.4
HRP-II	$(5.7 \pm 0.5) \times 10^2$	6.4, 7.4

*The values represent the mean ± SD from three to six independent stopped-flow experiments (Fig. 3, and Figs. S2, S3, and S4). The values obtained for HRP reactions at pH 6.4 and 7.4 did not differ significantly and the shown values are the mean ± SD of both sets of experiments.

Tempol Effects on Time-Dependent Substrate Consumption and Product Formation. In incubations containing MPO, almost all H_2O_2 (Fig. 4*B*) and less than half of the NO_2^- (Fig. 4*A*) were consumed in ≈5–10 min in the absence of tempol. Its presence completely inhibited NO_2^- consumption (Fig. 4*A*), whereas H_2O_2 consumption remained similar initially, but faster at late times (Fig. 4*B*). Formation of 3-nitrotyrosine in RNase was marginal in the presence of 10 μM tempol (Fig. 4*C*), in agreement with spent incubation mixture analysis (Fig. 1). The small effects of tempol on H_2O_2 consumption, compared with its pronounced inhibition of NO_2^- consumption and RNase nitration (Fig. 4), indicated that H_2O_2 was consumed in processes other than RNase oxidation/nitration. One possibility was H_2O_2 decomposition to O_2 (17, 18) and, indeed, tempol greatly increased O_2 evolution in the incubation mixtures (Fig. 4*D*). To ensure an accurate measurement of evolved O_2 whose solubility in aqueous solution is ≈0.2 mM, lower H_2O_2 concentrations (0.3 and 0.4 mM) were used in MPO-containing mixtures because they consumed all available peroxide (Fig. 4*D*). In the presence of tempol, evolved O_2 always accounted for approximately one fourth of consumed H_2O_2. By extrapolation, we estimated that 1 mM H_2O_2 would produce ≈0.25 mM O_2 (Fig. 4*D*). Similar effects of tempol were observed in HRP-containing incubations but substrate consumption and

product formation were much slower (Fig. S5) than in MPO-containing incubations (Fig. 4).

Kinetic Simulations. To obtain mechanistic insights about the inhibitory effect of tempol on MPO-mediated RNase nitration, kinetic simulations were performed with the Gepasi software (28) by using the reactions and corresponding rate constants listed in Table S1. A reasonable agreement was obtained between experimental and modeled variation of substrate and product concentrations with time (Fig. 4, black and red lines, respectively). The major discrepancy was in the concentration of evolved O_2. However, experimental evolved O_2 was obtained by extrapolation caused by limited O_2 solubility in aqueous solutions (Fig. 4*D*). In addition, many parallel reactions occur in MPO-containing incubations and several of the reported second-order rate constants were not obtained under our experimental conditions (Tables S1 and S2). Thus, the fit between experimental and modeled data can be considered reasonable and informative because it allowed us to test which of the many possible reactions and estimated second-order rate constants affected data simulation (Tables S1 and S2). Tempol reactions with MPO-I and MPO-II (Table 1) marginally affected data simulation and thus, are unlikely to play a significant role in inhibiting MPO-mediated RNase nitration. Likewise, tempol effects on HRP-mediated RNase nitration were reasonably modeled and were concluded to be independent of tempol reaction with HRP-I and HRP-II (data not shown).

Discussion

The substantial therapeutic potential of cyclic nitroxides as antioxidants has stimulated innumerous studies of their reaction with reactive oxygen species (5, 6). In comparison, reactions of nitroxides with $NO^{\bullet}$-derived oxidants have been less frequently investigated (7, 9–13). However, $NO^{\bullet}$-derived oxidants promote protein-tyrosine nitration (15), a protein posttranslational modification that is decreased in the injured tissues of animal models of inflammation on tempol administration (14). In particular, tempol effects on MPO-mediated protein-tyrosine nitration remained unexplored, although MPO is a crucial player in various infectious and inflammatory conditions (16, 19, 20). Our studies contribute to fill this hiatus.

We showed that tempol efficiently inhibits MPO-mediated RNase nitration, acting almost as a true catalyst (Fig. 1). Also, we showed that tempol reacts with MPO-I, MPO-II, HRP-I, and HRP-II with second-order rate constants (Table 1) that are orders of magnitude higher than that reported for ferryl-myoglobin ($1.6 \times 10^1\ M^{-1}\ s^{-1}$) (18). Nevertheless, the determined second-order constants were not exceptionally high, corroborating a previous inference that a tempol analogue was not a good substrate for peroxidases (29). Although a better substrate for MPO than HRP, the second-order rate constants of tempol reaction with MPO-I and MPO-II are in the range of those of endogenous metabolites, such as NO_2^- (30).

The second-order rate constant values of MPO-I and MPO-II reaction with NO_2^- at pH 5 (1.1×10^7 and $8.9 \times 10^4\ M^{-1}\ s^{-1}$, respectively) are considerable higher than at pH 7 (2.0×10^6 and $5.5 \times 10^2\ M^{-1}\ s^{-1}$, respectively) (30), and this should contribute to the higher yield of RNase nitration observed at acid pH (Fig. 1). However, EPR experiments showed that at least one RNase-tyrosine residue is highly exposed and reacts with MPO/H_2O_2 even in the absence of NO_2^- (Fig. 2). The better candidates are Tyr^{92} and Tyr^{76}, which are exposed (21) and became extensively modified on treatment with $MPO/H_2O_2/NO_2^-$ (Fig. S1). Reaction of MPO-I with RNase at pH 5.4 was confirmed by preliminary stopped-flow experiments from which a second-order rate constant with a magnitude similar to that reported for Tyr was estimated ($\approx 10^5\ M^{-1}\ s^{-1}$) (31). This rapid reaction is likely to be favored by RNase unfolding at acid pH (32). Even so, the relative

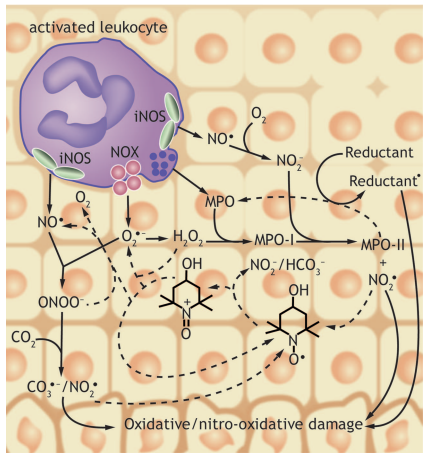

Fig. 5. Schematic representation of sources of $NO^{\bullet}$-derived oxidants and tempol reactions that may attenuate tissue injury in inflammatory conditions. The scheme presents an extremely simplified overview, where the oxidants are produced by activated leukocytes expressing inducible $NO^{\bullet}$ synthase (iNOS) and NOX (phagocyte NADPH oxidase), and extruding MPO. The reactions are not balanced, some intermediates have been omitted for clarity, and the possibility of the oxammonium cation ($TPNO^+$) being recycled by endogenous reductants has been omitted for lack of data (see text). Radicals produced from the oxidation of endogenous reductants by MPO or $TPNO^+$ may contribute to oxidative damage. Reactions downstream of $NO^{\bullet}$ and $O_2^{\bullet-}$ leading to oxidants capable of promoting tissue damage are marked with full lines, whereas protective reactions are marked with interrupted lines.

inaccessibility of the MPO active site argues for the participation of a MPO-surface-exposed amino acid radical, the so-called MPO-I isomer, in RNase oxidation (24–26). The possibility of MPO directly oxidizing protein residues at acidic pH, that is, without the assistance of other substrates, such as NO_2^- and Tyr, deserves further study because of its many pathophysiological implications (16, 19, 24, 26).

Mechanistic insights about the inhibitory effect of tempol on peroxidase-mediated RNase nitration was obtained by quantifying substrate consumption and product formation in the presence and absence of tempol and modeling the results by kinetic simulations (Fig. 4; Table S1). Tempol reactions with MPO-I and MPO-II (Table 1) marginally affected data simulation, excluding their significant role in inhibiting MPO-mediated RNase nitration. In fact, the inhibitory effects of tempol can be attributed mainly to its reaction with $NO_2^{\bullet}$ to produce the oxammonium cation, which, in turn, recycles back to tempol by reacting with H_2O_2 and $O_2^{\bullet-}$ to produce O_2 and recycle $NO_2^{\bullet}$ to NO_2^- (Fig. 5; Table S1, reactions 12, 13 and 14). Another relevant tempol reaction is with the RNase-$tyr^{\bullet}$ (Table S1, reaction 15) which consumes the nitroxide (Fig. 1*B*) and precludes its continuous recycling.

Thus, tempol inhibits MPO-mediated RNase nitration mainly because of its reaction with $NO_2^{\bullet}$. Although inferred from experiments performed with nonphysiological concentrations of NO_2^- and H_2O_2, the tempol inhibition mechanism should hold under physiological conditions. In fact, the second-order rate constants reported here, together with the available literature data, may be used to model a variety of hypothetical physiological conditions (Table 1; Tables S1 and S2).

Our studies add important information to unravel the mechanisms by which nitroxides attenuate the toxicity of $NO^{\bullet}$-derived oxidants, whose formation likely depends on reactions catalyzed by mammalian hemeperoxidases such as MPO and eosinophil peroxidase (EPO), among other mechanisms (Fig. 5). Recently, the peroxidase activity of prostaglandin endoperoxide H synthase (33) and the oxygenase domain of inducible $NO^{\bullet}$ synthase

(34) have been proposed to be additional sources of $NO_2^{\bullet}$ in mammals. Because MPO is a very reactive enzyme, our demonstration that tempol reacts with MPO-I and MPO-II at rates comparable to those of endogenous substrates should hold for other peroxidases. Except in cases of accentuated steric hindrance, the second-order rate constants we determined should also hold for many nitroxides because electronic structure and electron delocalization play minor roles in their reactions (35). The demonstration that the recombination reaction of tempol with protein-tyr$^{\bullet}$ is an important route for nitroxide consumption was also relevant. Nitroxide decay by recombination reactions with protein-thiyl (7) and glutathionyl-derived radicals (29) has been proposed. It has usually been assumed that reduction of nitroxide to the corresponding hydroxylamine is the main decay route for these compounds *in vivo*, but the contribution of recombination reactions deserves to be evaluated.

On the basis of this and previous work (7, 9–13), we propose that nitroxides attenuate the toxic effects of NO$^{\bullet}$-derived oxidants mainly because of their capability to react rapidly with $NO_2^{\bullet}$ and/or $CO_3^{\bullet-}$ ($k > 10^8$ M^{-1} s^{-1}) that would otherwise attack a variety of biological targets, including protein-tyrosine residues. In the process, the nitroxide is oxidized to the corresponding oxammonium cation, which may, in turn, be recycled back to the nitroxide by reacting with $NO_2^{\bullet}$ and $CO_3^{\bullet-}$ precursors such as peroxynitrite and H_2O_2 to produce upstream species such as NO$^{\bullet}$, $O_2^{\bullet-}$, and O_2 (Fig. 5). *In vivo*, it is likely that the oxammonium cation can be recycled by cellular reductants, but these reactions have yet to be explored (9). Because tempol is effective at reducing inflammatory injury in genuine physiological conditions, specifically in animal models, it is conceivable that nitroxide targeting to cells and sites of increased NO$^{\bullet}$-derived oxidant production may become a potential therapeutic strategy. A proof of the concept is found in the promising results obtained by targeting nitroxides to mitochondria and mitochondrial membranes to reduce oxygen-derived radical levels (6, 36).

Experimental Procedures

Materials. All commercial reagents were analytical grade or better. MPO from human leukocytes was purchased from Alexis Biochemicals and had an RZ (A_{430}/A_{280}) $\geq$ 0.75. MPO concentration and activity was determined spectrophotometrically ($\varepsilon_{430} = 8.9 \times 10^4$ M^{-1} cm^{-1} per heme) (37) and by the guaiacol oxidation assay (38), respectively. HRP was obtained from Sigma, and its concentration was determined spectrophotometrically ($\varepsilon_{401} = 1.02 \times 10^5$ M^{-1} cm^{-1}) (39). Solutions of H_2O_2 were prepared before use, and the concentration determined spectrophotometrically ($\varepsilon_{240} = 43.6$ M^{-1} cm^{-1}) (40). Tempol concentration was determined spectrophotometrically ($\varepsilon_{240} = 1.44 \times 10^3$ M^{-1} cm^{-1}) (41). Buffers were pretreated with Chelex-100 to remove transition metal ion contamination. All solutions were prepared with distilled water purified with a Millipore Milli-Q system.

Incubation Mixtures. Unless stated otherwise, the reaction mixtures contained 370 μM RNase, 1 mM H_2O_2, 1 mM NO_2^-, and either 30 nM (10 units/ml) MPO or 10 μM (450 units/ml) HRP in 50 mM phosphate, pH 5.4, 6.4, or 7.4, and were incubated at 37°C.

RNase Nitration. Total yield of RNase nitration was monitored by determining spectrophotometrically 3-nitrotyrosine formation ($\varepsilon_{430} = 4.4 \times 10^3$ M^{-1} cm^{-1}) (42). After the incubation time specified in the figure legends, the reactions were stopped by catalase addition (50 units/ml). Alternatively, the spent reaction mixtures were treated with trypsin and analyzed by HPLC (Fig. S1).

EPR Experiments. The EPR spectra were recorded at room temperature (25 ± 2°C) on a Bruker EMX instrument. The incubations were performed as described above except for the presence of tempol and/or DBNBS as specified in the legend to Fig. 2.

Hydrogen Peroxide Analysis. The concentration of H_2O_2 remaining in the reaction mixtures at different incubation times was determined by an iodometric assay as reported (43).

Nitrite Analysis. The concentration of NO_2^- remaining in the reaction mixtures at different incubation times was determined on a chemiluminescence NO analyzer (NOA^{TM280}, Sievers Instruments). Aliquots were taken from the incubation mixtures, diluted (1:50), and reduced in the analyzing cell with saturated NaI solution in 50% acetic acid (7).

Oxygen Evolution. Evolved O_2 was monitored on an oxygen monitor (Gilson 5/6 oxygraph). The instrument was calibrated by the amount of O_2 evolved after addition of catalase (50 units/ml) to H_2O_2 standard solutions.

Kinetic Studies. They were performed in a stopped-flow spectrophotometer (Applied Photophysics SX-18MV) at 25.0 ± 0.5°C by using the sequential mixing mode. In the reaction of MPO-I with tempol, 0.2 μM MPO was premixed with 4 μM H_2O_2 in 0.1 M phosphate buffer, pH 7.4. After a delay time of 0.1 s, formed MPO-I was allowed to react with varying concentrations of tempol that were at least 10-fold in excess of MPO-I (29), but not too high to preclude the attainment of steady-state conditions. The reaction course was monitored by absorbance changes at 456 nm that accompany the formation of MPO-II; this wavelength is the isosbestic point between MPO and MPO-I (37). In the reaction of MPO-II with tempol, it was impossible to employ the usual procedure of preincubating MPO with a 50-fold excess of H_2O_2 (31) because preliminary experiments and kinetic simulations showed that steady-state conditions were attained too quickly, precluding rate measurements. Thus, 0.2 μM MPO was premixed with equimolar H_2O_2 in phosphate buffer (24). After a delay time of 0.5 s, the formed MPO-I was allowed to react with varying concentrations of tempol in at least 10-fold excess, and the reaction course was monitored at 456 nm as above in two time frames (24). First, the fast reaction of MPO-I with tempol to quantitatively produce MPO-II was monitored. Subsequently, MPO-II decay by reaction with high-excess tempol was monitored in a slower time frame. HRP reactions were slower and the usual kinetic approaches were used. In these cases, HRP (2.5–3 μM) was premixed with equimolar H_2O_2 in 0.1 M phosphate buffer, pH 7.4 or 6.4. After a delay time of 1 s, the formed HRP-I was allowed to react with varying concentrations of tempol and the reaction course was monitored by formation of HRP-II at 411 nm, the isosbestic point between HRP-II and HRP. In the reaction of HRP-II, 3 μM HRP and 3 μM ferrocyanide were premixed with 3 μM H_2O_2 in 0.1 M phosphate buffer, pH 7.4 or 6.4. After a delay time of 2.5 s, the formed HRP-II was allowed to react with varying concentrations of tempol. The reaction course was monitored by the decay of HRP-II at 425 nm (44). In all cases, k_{obs} values were determined by using the single curve-fit equation of the instrument software. Three to six determinations of k_{obs} were performed for each substrate concentration. The apparent second-order rate constants were calculated from the slopes by using linear least-squares regression analysis.

Kinetic Simulations. Kinetic simulations were performed with the Gepasi 3.30 software (http://gepasi.dbs.aber.ac.uk/softw.html/) (28).

ACKNOWLEDGMENTS. We thank Prof. Peter Wardman for the discussion of second-order rate constant values, and Maria L. V. Pereira for the artwork in Fig. 5. This work was supported by grants from Fundação de Amparo à Pesquisa do Estado de São Paulo (FAPESP) and Conselho Nacional de Desenvolvimento Científico e Tecnológico (CNPq) (Projeto Institutos do Milênio: Redoxoma).

1. Brennan ML, Hazen SL (2003) Amino acid and protein oxidation in cardiovascular disease. *Amino Acids* 25:365–374.
2. Kris-Etherton PM, Lichtenstein AH, Howard BV, Steinberg D, Witztum JL (2004) Antioxidant vitamin supplements and cardiovascular disease. *Circulation* 110:637–641.
3. Szabo C, Ischiropoulos H, Radi R (2007) Peroxynitrite: Biochemistry, pathophysiology and development of therapeutics. *Nat Rev Drug Discov* 6:662–680.
4. Augusto O, *et al.* (2002) Nitrogen dioxide and carbonate radical anion: Two emerging radicals in biology. *Free Radical Biol Med* 32:841–859.
5. Soule BP, *et al.* (2007) The chemistry and biology of nitroxide compounds. *Free Radical Biol Med* 42:1632–1650.
6. Kagan VE, Jiang J, Bayir H, Stoyanovsky DA (2007) Targeting nitroxides to mitochondria: location, location, location, and concentration: Highlight commentary on "Mitochondria superoxide dismutase mimetic inhibits peroxide-induced oxidative damage and apoptosis: role of mitochondrial superoxide." *Free Radical Biol Med* 43:348–350.
7. Fernandes DC, Medinas DB, Alves MJ, Augusto O (2005) Tempol diverts peroxynitrite/carbon dioxide reactivity toward albumin and cells from protein-tyrosine nitration to protein-cysteine nitrosation. *Free Radical Biol Med* 38:189–200.
8. Krishna MC, Grahame DA, Samuni A, Mitchell JB, Russo A (1992) Oxoammonium cation intermediate in the nitroxide-catalyzed dismutation of superoxide. *Proc Natl Acad Sci USA* 89:5537–5541.

9. Goldstein S, Merenyi G, Russo A, Samuni A (2003) The role of oxoammonium cation in the SOD-mimic activity of cyclic nitroxides. *J Am Chem Soc* 125:789–795.
10. Bonini MG, Mason RP, Augusto O (2002) The mechanism by which 4-hydroxy-2,2,6,6-tetramethylpiperidene-1-oxyl (tempol) diverts peroxynitrite decomposition from nitrating to nitrosating species. *Chem Res Toxicol* 15:506–511.
11. Goldstein S, Samuni A, Russo A (2003) Reaction of cyclic nitroxides with nitrogen dioxide: The intermediacy of the oxammonium cations. *J Am Chem Soc* 125:8364–8370.
12. Goldstein S, Samuni A, Merenyi G (2004) Reactions of nitric oxide, peroxynitrite, and carbonate radicals with nitroxides and their corresponding oxoammonium cations. *Chem Res Toxicol* 17:250–257.
13. Goldstein S, Samuni A, Hideg K, Merenyi G (2006) Structure-activity relationship of cyclic nitroxides as SOD mimics and scavengers of nitrogen dioxide and carbonate radicals. *J Phys Chem A* 110:3679–3685.
14. Thiemermann C (2003) Membrane-permeable radical scavengers (tempol) for shock, ischemia-reperfusion injury, and inflammation. *Crit Care Med* 31:S76–S84.
15. Radi R (2004) Nitric oxide, oxidants, and protein tyrosine nitration. *Proc Natl Acad Sci USA* 101:4003–4008.
16. Arnhold J, Furtmüller PG, Obinger C (2003) Redox properties of myeloperoxidase. *Redox Rep* 8:179–186.
17. Mehlhorn RJ, Swanson CE (1992) Nitroxide-stimulated H_2O_2 decompositions by peroxidases and pseudoperoxidases. *Free Radical Res Commun* 17:157–175.
18. Krishna MC, Samuni A, Taira J, Goldstein S, Mitchell JB, Russo A (1996) Stimulation by nitroxides of catalase-like activity of hemeproteins. Kinetics and mechanism. *J Biol Chem* 271:26018–26025.
19. Nicholls SJ, Hazen SL (2005) Myeloperoxidase and cardiovascular disease. *Arterioscler Thromb Vasc Biol* 25:1102–1111.
20. Furtmuller PG, *et al.* (2006) Active site structure and catalytic mechanisms of human peroxidases. *Arch Biochem Biophys* 445:199–213.
21. Souza JM, Daikhin E, Yudkoff M, Raman CS, Ischiropoulos H (1999) Factors determining the selectivity of protein tyrosine nitration. *Arch Biochem Biophys* 371:169–178.
22. Wright PJ, English AM (2002) Scavenging with TEMPO• to identify peptide- and protein-based radicals by mass spectrometry: Advantages of spin scavenging over spin trapping. *J Am Chem Soc* 125:8655–8665.
23. Davies MJ, Hawkins CL (2004) EPR spin trapping of protein radicals. *Free Radical Biol Med* 36:1072–1086.
24. Tien M (1999) Myeloperoxidase-catalysed oxidation of tyrosine. *Arch Biochem Biophys* 367:61–66.
25. Lardinois OM, Ortiz de Montellano PR (2000) EPR spin-trapping of a myeloperoxidase protein radical. *Biochem Biophys Res Commun* 270:199–202.
26. Ghibaudi E, Laurenti E (2003) Unraveling the catalytic mechanism of lactoperoxidase and myeloperoxidase. A reflection on some controversial features. *Eur J Biochem* 270:4403–4412.
27. Jantschko W, *et al.* (2002) Redox intermediates of plant and mammalian peroxidases: A comparison transient kinetic study of their reactivity toward indole derivatives. *Arch Biochem Biophys* 398:12–22.
28. Mendes P (1997) Biochemistry by numbers: Simulation of biochemical pathways with GEPASI 3. *Trends Biochem Sci* 22:361–363.
29. Borisenko GG, *et al.* (2004) Glutathione propagates oxidative stress triggered by myeloperoxidase in HL-60 cells. Evidence for glutathionyl radical-induced peroxidation of phospholipids and cytotoxicity. *J Biol Chem* 279:23453–23462.
30. Burner U, Furtmüller PG, Kettle AJ, Koppenol WH, Obinger C (2000) Mechanism of reaction of myeloperoxidase with nitrite. *J Biol Chem* 275:20597–20601.
31. Marquez LA, Dunford HB (1995) Kinetics of oxidation of tyrosine and dityrosine by myeloperoxidase compounds I and II. *J Biol Chem* 270:30434–30440.
32. Roberts GC, Benz FW (1973) Proton Fourier transform NMR studies of the unfolding of ribonuclease. *Ann N Y Acad Sci* 222:130–148.
33. Palazzolo-Ballance AM, Suquet C, Hurst JK (2007) Pathways for intracellular generation of oxidants and tyrosine nitration by a macrophage cell line. *Biochemistry* 46:7536–7548.
34. Marechal A, Mattioli TA, Stuehr DJ, Santolini J (2007) Activation of peroxynitrite by inducible nitric-oxide synthase: A direct source of nitrative stress. *J Biol Chem* 282:14101–14112.
35. Novak I, Harrison LJ, Kovac B, Pratt LM (2004) Electronic structure of persistent radicals: nitroxides. *J Org Chem* 69:7628–7634.
36. Dhanasekaran A, *et al.* (2005) Mitochondria superoxide dismutase mimetic inhibits peroxide-induced oxidative damage and apoptosis: role of mitochondrial superoxide. *Free Radical Biol Med* 39:567–583.
37. Marquez LA, Huang JH, Dunford HB (1994) Spectral and kinetic studies on the formation of myeloperoxidase compounds I and II: Roles of hydrogen peroxide and superoxide. *Biochemistry* 33:1447–1454.
38. Klebanoff SJ, Waltersdorph A, Rosen H (1984) Antimicrobial activity of myeloperoxidase. *Methods Enzymol* 105:399–403.
39. Schannon LM, Kay E, Lew JL (1966) Peroxidase isozymes from horseradish roots. I. Isolation and physical properties. *J Biol Chem* 241:2166–2172.
40. Beers RJ, Sizer IW (1952) A spectrophotometric method for measuring the breakdown of hydrogen peroxide by catalase. *J Biol Chem* 195:133–140.
41. Hoffman BM, Eames TB (1969) Protonated nitroxide free radical. *J Am Chem Soc* 91:2169–2170.
42. Sampson JB, Ye Y, Rosen H, Beckman JS (1998) Myeloperoxidase and horseradish peroxidase catalyze tyrosine nitration in proteins from nitrite and hydrogen peroxide. *Arch Biochem Biophys* 356:207–213.
43. Hochanadel CJ (1952) Effects of cobalt γ-radiation on water and aqueous solutions. *J Phys Chem* 56:587–594.
44. Ralston IM, Dunford HB (1980) Horseradish peroxidase. XLII. Oxidations of L-tyrosine and 3,5-diiodo-L-tyrosine by compound II. *Can J Biochem* 58:1270–1276.